Applied Physics A (2021) 127:627
https://doi.org/10.1007/s00339-021-04748-7

Applied Physics A
Materials Science & Processing

Synthesis and characterization of cobalt molybdate dihydrate nanorods arrays for supercapacitor electrode application

G. Harichandran[1] · S. Radha[1] · J. Yesuraj[2] · B. Muthuraaman[2]

Received: 24 May 2021 / Accepted: 7 July 2021 / Published online: 26 July 2021

Abstract
In this endeavor, cobalt molybdate dihydrate materials were synthesized by CTAB assisted hydrothermal method and this material was utilized as electrode materials for supercapacitor application. X-ray diffraction analysis, Fourier transform infrared spectroscopic and Raman spectral analyses confirmed the formation of cobalt molybdate dihydrate materials. CTAB was used to tune the morphological features of the cobalt molybdate dihydrate materials. The nanorod arrays (COM-4 material) were formed when a high concentration of CTAB template was used during the synthesis. The supercapacitor features of the prepared materials were characterized using cyclic voltammetric (CV), galvanostatic charge/discharge (GCD) analysis in 1 M KOH electrolyte. The CV curves confirm the pseudocapacitive nature and provide the specific capacitance of 768 Fg^{-1} at a scan rate of 5 mVs^{-1} whereas the GCD curves offer the specific capacitance of 796 Fg^{-1} at a current density of 1 Ag^{-1}. The stability test established the capacitance retention of about 95% after 2000 continuous CV cycles at a scan rate of 100 mVs^{-1}. These findings suggested the significant usage of cobalt molybdate dihydrate materials in energy storage devices.

Keywords Cobalt molybdate dihydrate · Supercapacitors · Energy storage · Hydrothermal · CTAB

1 Introduction

Environmental problems such as pollution, global warming, and high usage of fossil fuels are required to generate energy from sustainable and renewable energy sources [1]. Though, effective and consistent energy storage devices are necessary for the effective utilization of renewable clean energy sources. Supercapacitors are regarded as a competent energy storage device when compared to other clean energy storage devices such as batteries and fuel cells because it is practicable, eco-friendly and sustainable nature. Supercapacitors with favorable features such as rapid charge–discharge progression, the high value of power density, superior cycle stability, compact size are regarded as propitious applicants for energy storage technologies of the next decade [2–5]. Electrochemical double-layer capacitors (EDLC) and pseudocapacitors are the two major categories of supercapacitors, which are separated based on the energy storage process. The EDLC stores energy through the process of charge separation at the interface between electrode and electrolyte, whereas pseudo-capacitors stores energy on the surface of electrode materials through a faradaic redox reaction. Numerous research efforts have been devoted to pseudocapacitor device since it exhibits high energy density than EDLC's [6, 7].

The $NiMoO_4$ [8], $CoMoO_4$ [9] and $MnMoO_4$ [10] are some of the binary transition metal molybdates, which have recently been investigated for supercapacitor application as their feasible properties like easy abundant, cost-effective and eco-friendly nature. Due to variable oxidation states and superior electrical conductivity, the metal molybdates have been shown to exhibit efficient electrochemical features than single transition metal oxides. Among them, $CoMoO_4$ is a significant candidate for supercapacitor application since it consists of two transition metal oxides (cobalt and molybdenum oxides) with high specific capacitances and superior long cycle life. Therefore, combining the favorable characteristics of cobalt and molybdenum oxides could strengthen the capacitive properties [9]. Various kinds of literature are available on $CoMoO_4$ as a supercapacitor electrode material.

✉ G. Harichandran
umghari@gmail.com

[1] Department of Polymer Science, University of Madras, Guindy Campus, Chennai 600 025, India

[2] Department of Energy, University of Madras, Guindy Campus, Chennai 600 025, India

For Example, Hou, et al. [11] demonstrated ultrafine $CoMoO_4 \cdot 0.9H_2O$ nanorods, achieved by hydrothermal synthetic technique with the assistance of various templates. The $CoMoO_4 \cdot 0.9H_2O$ nanorods provide 377 Fg^{-1} of specific capacitance and retained 93% of initial specific capacitance after 1000 cycles at a scan rate of 0.5 Ag^{-1}. Li et al. [12] also established the $CoMoO_4$ microspheres via the hydrothermal synthetic method which exhibits 186 Fg^{-1} of specific capacitance and possesses excellent cyclic stability up to 1000 cycles at 8 Ag^{-1}. In addition, Long et al. [13] synthesized 3D-frameworks contain $CoMoO_4$ nanosheets which offer 1234 Fg^{-1} of specific capacitance at 1 Ag^{-1} and exhibit long cyclic stability till 5000 continuous cycles. Wang et al. [14] synthesized both $CoMoO_4$ nanowires covered $CoMoO_4$ nanosheets through the water bath heating process which provide the specific capacitance of 1960 Fg^{-1} at 1 Ag^{-1} with a rating feature of 64% and exhibits 98.79% capacitance retention subsequently 10,000 cycles. The outcomes of the reported electrochemical analysis indicate that the ability charge storage performance depends largely on the morphology of electrode materials. Consequently, much effort is needed to alter the morphologies of the electrode materials to attain high specific capacitance for future energy storage devices.

Present endeavor, the nanorod-shaped cobalt molybdate dihydrate materials were prepared through facile CTAB assisted hydrothermal technique. The XRD, FTIR and Raman experimental techniques confirm the formation of cobalt molybdate dihydrate materials. The electrochemical tests proposed that the nanorod-shaped cobalt molybdate dihydrate electrode study the specific capacitance and excellent rate capability. Moreover, the advantage of hydrothermal synthetic method facile, calcination-free process provides highly principle-oriented nanostructures were presented.

2 Materials and methods

2.1 Materials

Analar grade of cobalt acetate tetrahydrate ($Co(CH_3COO)_2.4H_2O$), sodium molybdate dihydrate ($Na_2MoO_4.2H_2O$), sodium hydroxide and hydrochloric acid (HCl) were procured from Sisco Research Laboratories Pvt. Ltd. (India). In addition, N-methyl-2-pyrrolidone (NMP), Carbon black, and polyvinylidene difluoride (PVDF) were obtained from Loba Chemie Pvt. Ltd. (India). Potassium hydroxide and nickel foil (0.025 mm thickness), 99.5% (metal basis) were purchased from Alfa-Aesar (India). Double distilled water was utilized for all the tests and preparations.

2.2 Experimental section

2.2.1 Synthesis of cobalt molybdate materials

Cobalt acetate tetrahydrate and sodium molybdate dihydrate have been selected as the precursor materials to synthesize cobalt molybdate materials in a typical procedure. About equimolar (0.07 M) quantities of sodium molybdate and cobalt acetate dihydrate crystals had been separately made to dissolve in 40 ml of double-distilled water using a magnetic stirrer which stirred at a speed of 400 rpm. The sodium molybdate solution was mixed slowly in a dropwise manner to the cobalt acetate solution, meanwhile stirring was also continued for another 30 min. The pH of the solution was maintained to ~10 using 1 M sodium hydroxide solution and the temperature of the mixture was raised to 70 °C while stirring. Ultrasonication of the resultant homogeneous mixture had been accomplished with an ultrasonic cleaner of type orchid scientific, model PS-500 for 30 min at room temperature. After carrying out the ultrasonication, the mixture was transferred to Teflon lined autoclave and heated to 180 °C for 24 h by keeping that in the furnace. The formed cobalt molybdate material had been washed many times with double distilled water, filtered and dried to 70 °C in a hot air oven for 12 h. The synthesized material was named COM-1. To improve the morphology of the as-synthesized cobalt molybdate, duplicate experiments had also been performed by changing the CTAB concentration to 1 M, 2 M and 3 M and the prepared materials were labeled as COM-2, COM-3 and COM-4, respectively.

2.2.2 Characterizations

The PANalytical X-pert PRO diffractometer with Cu-Kα radiation ($\lambda = 0.154060$ nm, 40 kV and30 mA) at a scan rate of 0.07° s^{-1} was used to record X-ray diffraction (XRD) patterns for prepared cobalt molybdate dihydrate materials whereas Perkin-Elmer RX1'spectrophotometer (with 4 cm^{-1} resolution for 20 scans) was used to analyze Fourier transform infrared (FTIR) spectroscopy. Raman spectral analyses of the cobalt molybdate dihydrate samples were assessed using Confocal Raman (I-11 Model) spectrophotometer, Nanophoton Corp., which uses laser rays (532 nm), produced from Argon laser source. The spectral data have been recorded in the range of 2000–250 cm^{-1}. The high-resolution transmission electron microscope (HRTEM, Techni G2S-TWIN, FEI) was employed to analyze morphological characteristics.

2.2.3 Electrode preparation

Three electrode configurations were employed to analyze the electrochemical properties of freshly prepared cobalt molybdate dihydrate material in a 1 M KOH electrolyte. Platinum

wire and saturated calomel electrode were utilized as counter and reference electrodes, respectively. The working electrode was fabricated using active material, carbon black and poly (vinylidene fluoride) (PVDF) with a ratio of 80:10:10. The slurry was made using above-mentioned materials with the assistance of N-methyl pyrrolidone (NMP) solvent and then it was coated on the nickel foil. The active material-coated nickel foil was dried in a vacuum oven at 60 °C for 24 h and the final mass of the active materials was approximately 4 mg. Moreover, Cyclic voltammetric (CV) and galvanostatic charge/discharge (GCD) techniques were employed to analyze supercapacitor properties using a Biologic (SP-150 model) instrument.

3 Results and discussions

The crystal phase of the materials and structural details were evaluated using XRD spectra. Figure 1a–d shows the XRD pattern of all the cobalt molybdate hydrate materials. Speciously, all the obtained Bragg reflection bands can be dispensed to the cobalt molybdate dihydrate ($CoMo_4O_{13}(H_2O)_2$) phase with the JCPDS card no: 98-012-0397.The diffraction peaks obtained at 23, 25.2, 26.3, 26.4, 27.5, 28.6, 32.5, 33.2, 36.3, 38.8, 40.2, 41.7, 43.2, 45.1 47.2, 52, 53.3, 54.5, 55.5, 58.2, 60.2, 63.2 and 64.6 are corresponding to (101), (020), (1-11), (111), (01-2), (1-1-2), (20-1), (102), (10-3), (201), (03-1), (22-1), (20-3), (2-1-3), (202), (1-23), (04-1), (2-1-4), (2-31), (320), (1-33), (1-3-4) and (03-4) planes, respectively. The absence of impurity peaks confirms the formation of highly pure cobalt molybdate dihydrate material.

The bonding structure of prepared cobalt molybdate dihydrate is analyzed by FTIR analysis as shown in Fig. 2. The peaks located at 927, 841, 783, 711, 647, 530 cm^{-1} are resembling the formation of cobalt molybdate materials. The peaks that appeared from 927 to 711 cm^{-1} are assigned to Mo–O stretching bands. The band visible at 647 cm^{-1} is ascribed to the stretching vibration of Mo–O–Mo in cobalt molybdate dihydrate materials. The peak at 530 cm^{-1} is due to Co and Mo building blocks of $CoMoO_4$. The peaks at 3360 and 1630 cm^{-1} are corresponding to water molecules, respectively [15–18]. Further, Raman spectra support the nature of bonding in cobalt molybdate dihydrate material. Figure 4a–d represents the Raman spectra of the electrode materials namely COM-1, COM-2, COM-3 and COM-4, respectively. The peaks were observed between the regions 300–400 cm^{-1} and 800–900 cm^{-1} in the Raman spectrum. The bands visible at 928, 868, 810, 361 and 334 cm^{-1} could be assigned to cobalt molybdate specimens. Raman spectra of COM-1, COM-2, COM-3 and COM-4 include a strong band at 928 cm^{-1} weaker bands at 868 & 810 cm^{-1} and broad bands around 350 cm^{-1}. The broadband (around 350 cm^{-1}), a weak band (868 cm^{-1}) and a strong band (928 cm^{-1}) denote the Co–O–Mo stretching vibrations of the cobalt molybdate dihydrate materials [19, 20].

The surface morphologies of COM-1, COM-2, COM-3 and COM-4 materials were evaluated HR-TEM to explore

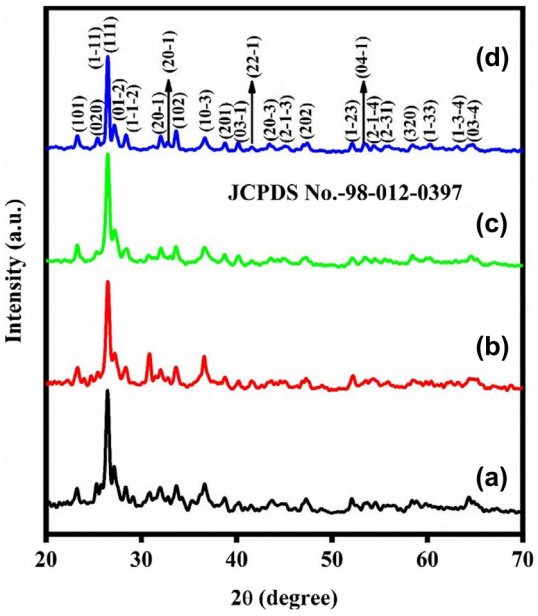

Fig. 1 XRD pattern of cobalt molybdate dihydrate materials; **a** COM-1; **b** COM-2; **c** COM-3 and **d** COM-4

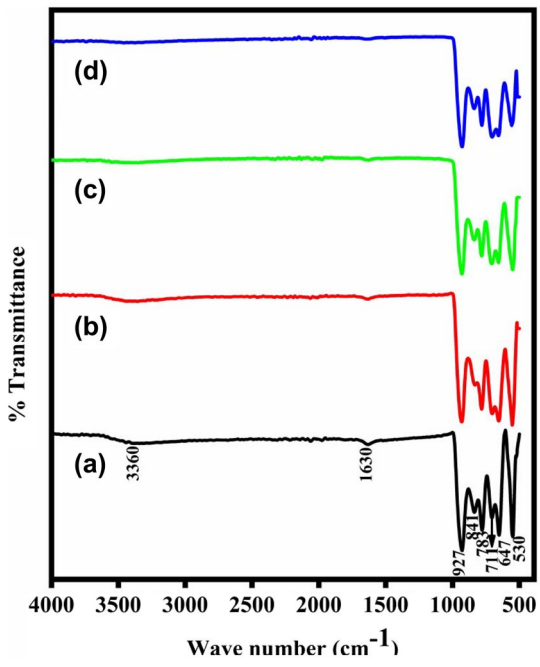

Fig. 2 FTIR spectra of cobalt molybdate dihydrate materials; **a** COM-1; **b** COM-2; **c** COM-3 and **d** COM-4

the effects of template variation in cobalt molybdate dihydrate materials as shown in Fig. 3. Figure 3a and b shows that lower and higher magnification images of COM-1 material which shows the micro size materials. In COM-2 (Fig. 3c and d) materials, the shaped materials are formed which is due to the inclusion of 1 mM of CTAB template. When the concentration of the CTAB template increased to 2 mM (COM-3), rod-shaped materials are formed. The shaped particles are also formed instead of rod-shaped materials as shown in Fig. 3e and f. The nanorod arrays are formed in COM-4 material (Fig. 3g), which was prepared using 3 mM of CTAB template. The high magnification image (Fig. 3h) shows that single nanorods which confirm that the single nanorods are formed initially and then it was arranged as nanorod arrays. These results are confirmed that the CTAB template and hydrothermal reaction condition are more effective for the formation of nanorod arrays. Figure 3i shows the fringes of the COM-4 materials which exhibit the interplanar d spacing of 3.8 Å corresponds to the (101) plane. The selected area electron diffraction (SAED) pattern of the COM-4 (Fig. 3g) material provides the d spacing which was measured to be approximately 3.8 and 3.3 Å ascribed to the (101) and (111) crystallographic planes, respectively. These outcomes are more comparable with the XRD results.

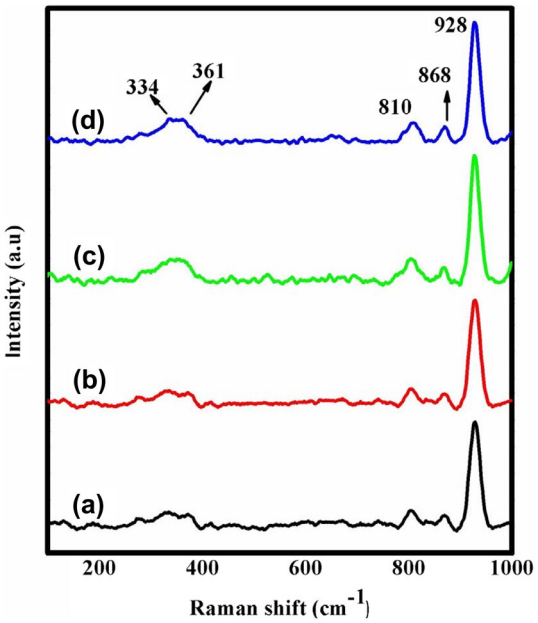

Fig. 3 Raman spectra of cobalt molybdate dihydrate materials; **a** COM-1; **b** COM-2; **c** COM-3 and **d** COM-4

3.1 Electrochemical supercapacitor analysis

The assessment of supercapacitor properties was done using CV and GCD techniques. First, the CV performance of all cobalt molybdate dihydrate was evaluated using 1 M KOH and shown in Fig. 4a–d. The potential window was fixed from −0.1 to 0.55 V at the scan rates from 5 to 100 mVs^{-1}. The redox pairs are completely exhibited in all the CV curves confirms the charge storage is followed the pseudocapacitor mechanism. The redox peaks are originated from the Co^{2+}/Co^{3+} charge transfer kinetics. In addition, the molybdate enhances the conductivity of $CoMoO_4$ materials and it is not involved in the redox process [21]. These redox peaks keep the original form, at a high scan rate of 100 mVs^{-1}, confirm to the high stability and quick moving of ions and

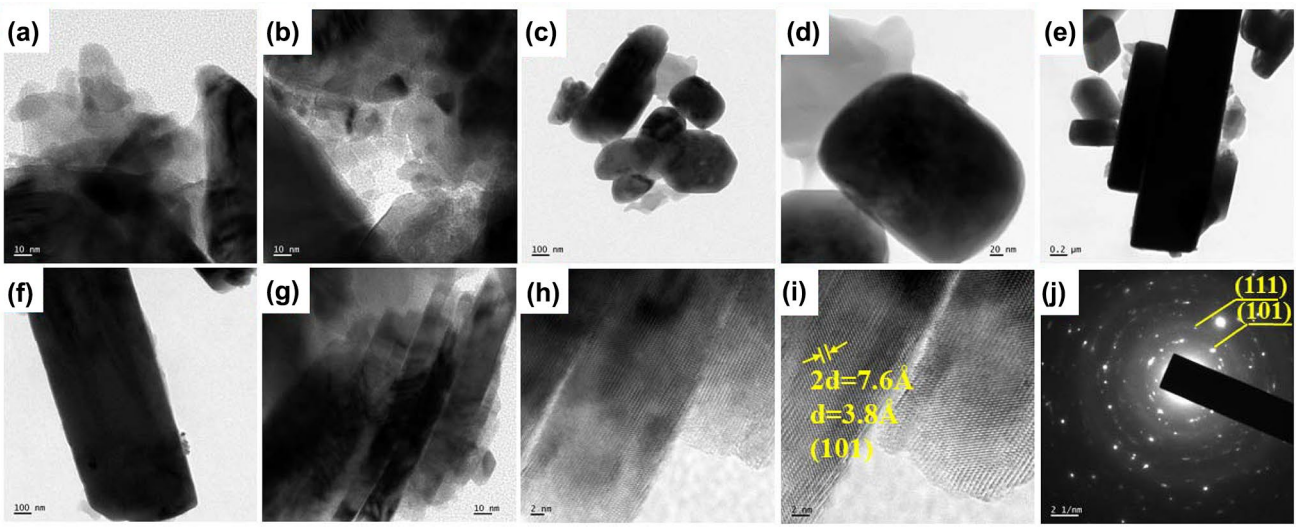

Fig. 4 HR-TEM images of cobalt molybdate dihydrate materials; **a**&**b** COM-1; **c** & **d** COM-2; **e** & **f** COM-3 and **g** & **h** COM-4; **i** fringes of COM-4 and **j** SAED pattern of COM-4 material

electrons in the cobalt molybdate dihydrate materials. In all the electrodes, the peak current increases with raising scan rate from 5 to 100 mVs^{-1} which ascribed to good reversibility of electrode materials [22]. Figure 4e shows the CV curves COM-1, COM-2, COM-3 and COM-4 electrodes at a scan rate of 5 mVs^{-1}. When compared with all electrodes, the COM-4 electrode exhibits a high surface area under the CV curve indicates the specific capacitance behavior. Besides, the specific capacitances of CV response can be calculated using Eq. (1) [21].

$$Csp = \frac{\int idV}{S.\Delta V.m} \tag{1}$$

where *Csp,* $\int idV$, ΔV, *m* and *S* denote the specific capacitance, integral area of CV curve, potential window (*V*), the mass of the active material (mg), and scan rate (mVs^{-1}), respectively. The specific capacitances of COM-1, COM-2, COM-3 and COM-4 electrodes are 207, 303, 681 and 768 Fg^{-1} at a scan rate of 5 mVs^{-1}, respectively. The specific capacitance vs scan rate graph is shown in Fig. 4f. The specific capacitance decreased when raising the scan rate from 5 to 100 mVs^{-1}. Due to fast scan, the electrolyte ions utilize only outer electrode materials for the electrochemical reaction which provide lower specific capacitance whereas the electrolyte ions can easily access both inner and outer region of electrode materials due to sufficient time, which offers high specific capacitance [23].

GCD analyses were performed to demonstrate an original capacitive behavior of the electrode materials. The CP curves COM-4 were recorded within a potential limit from −0.1 to 0.4 V at a current density of 1, 2, 3, 4, 5 and 10 Ag^{-1} as shown in Fig. 5. The GCD curves show good symmetry designates high reversibility and specific capacitive behavior of COM-4 electrodes. The CP curves also exhibit slight redox behavior confirming pseudocapacitive nature which is more comparable with CV analyses. From the GCD curves, the specific capacitance was calculated using Eq. (2) [24].

$$Csp = \frac{I\Delta t}{m\Delta V} \tag{2}$$

where Δt, ΔV, *m* and *I* denote the discharge time (*s*), potential window (*V*), the mass of the active material (mg), and discharge current density *(A)*, respectively. The discharge specific capacitance of 796, 752, 606, 424, 250 and 180 Fg^{-1} were obtained at 1, 2, 3, 4, 5 and 10 Ag^{-1}, respectively. The charging specific capacitance of 900, 812, 732, 520, 300 220 were attained 1, 2, 3, 4, 5 and 10 Ag^{-1}, respectively. The high discharge specific capacitance such as 796 Fg^{-1} is higher than earlier published results such as $CoMoO_4{\cdot}0.9H_2O$ nanorods (377 Fg^{-1}) [11], $CoMoO_4$ microspheres (186 Fg^{-1}) [12], $CoMoO_4$ material (259 Fg^{-1}) [25], $CoMoO_4$ nanorods (420 Fg^{-1}) [24] and $CoMoO_4$ nanomaterials(294 Fg^{-1}) [17].

The superior specific capacitance property of the COM-4 electrode is due to its nanorods array structure. It is well known that the nanorods provide a high surface area for electrochemical reaction and improved charge transport properties which enhance the specific capacitance. In addition, the nanorods arrays provide the continuation for the electrolyte ion moving which enhances the utilization of the more active materials during electrochemical analysis. Figure 5b shows the specific capacitance versus current density graph. The specific capacitance was decreased with increasing scan rate which is the same trend obtained in the CV profile. Equation 3 was used to calculate the coulombic efficiency of cobalt molybdate electrodes using charge/discharge curves:

$$\eta = \frac{\Delta t_d}{\Delta t_c} \times 100 \tag{3}$$

where η is coulombic efficiency (%), Δt_d is discharge time and Δt_c charging time. The coulombic efficiency of $NiCo_2O_4$-4 electrode is 97.6% at a current density of 10 A g^{-1}.

A cyclic stability study was performed to evaluate the stability feature of COM-4 material. The cyclic stability was recorded for continuous 2000 cycles at a scan rate of 100 mVs^{-1} and it is shown in Fig. 6. The initial specific capacitance is gradually decreased which is due to aggregation, dissolution, and the volume change arisen in the COM-4 electrode and it finally retained 95% of initial capacitance after 2000 cycles is shown in Fig. 7. This trend suggests that present COM-4 nanorod arrays possessing high stability. The high specific capacitance, good rate capability, superior cyclic stability features demonstrate the cobalt molybdate dihydrate (COM-4) nanorods arrays is a promising material for energy storage devices.

4 Conclusion

In this endeavor, the cobalt molybdate dihydrate nanorod arrays were successfully prepared by a CTAB assisted hydrothermal technique. The structural features bonding nature and surface morphological properties were briefly examined using XRD, FTIR and HR-TEM analyses. The CV and GCD studies demonstrated that the freshly prepared cobalt molybdate dihydrate materials exhibit a pseudocapacitor energy storage mechanism. The cobalt molybdate dihydrate nanorods arrays (COM-4) provide maximum specific capacitance of 796 Fg^{-1} from chronopotentiometry analysis at a current density of 1 Ag^{-1}, whereas the cyclic voltammetric curves offer the specific capacitance of 768 Fg^{-1} at a scan rate of 5 mVs^{-1}. The cyclic stability studies show that only 5% of degradation occurs till 2000 continuous CV cycles at a high scan rate of 100 mVs^{-1}. The high specific

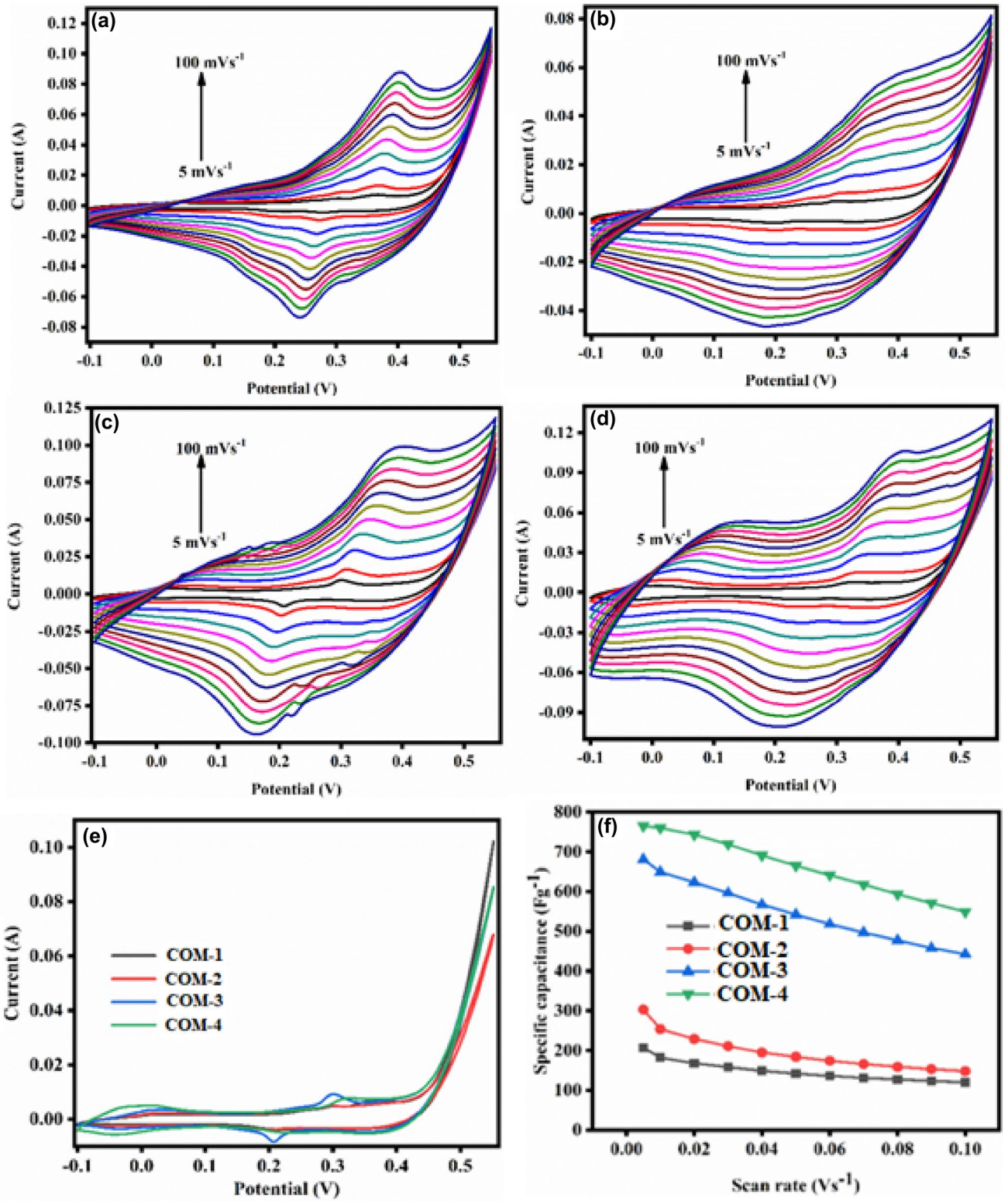

Fig. 5 Cyclic voltammetric analyses of cobalt molybdate dihydrate materials; **a** COM-1; **b** COM-2; **c** COM-3; **d** COM-4; **e** CV curves of all cobalt molybdate dihydrate materials at a scan rate of 5 mVs^{-1} and **f** Scan rate versus specific capacitance

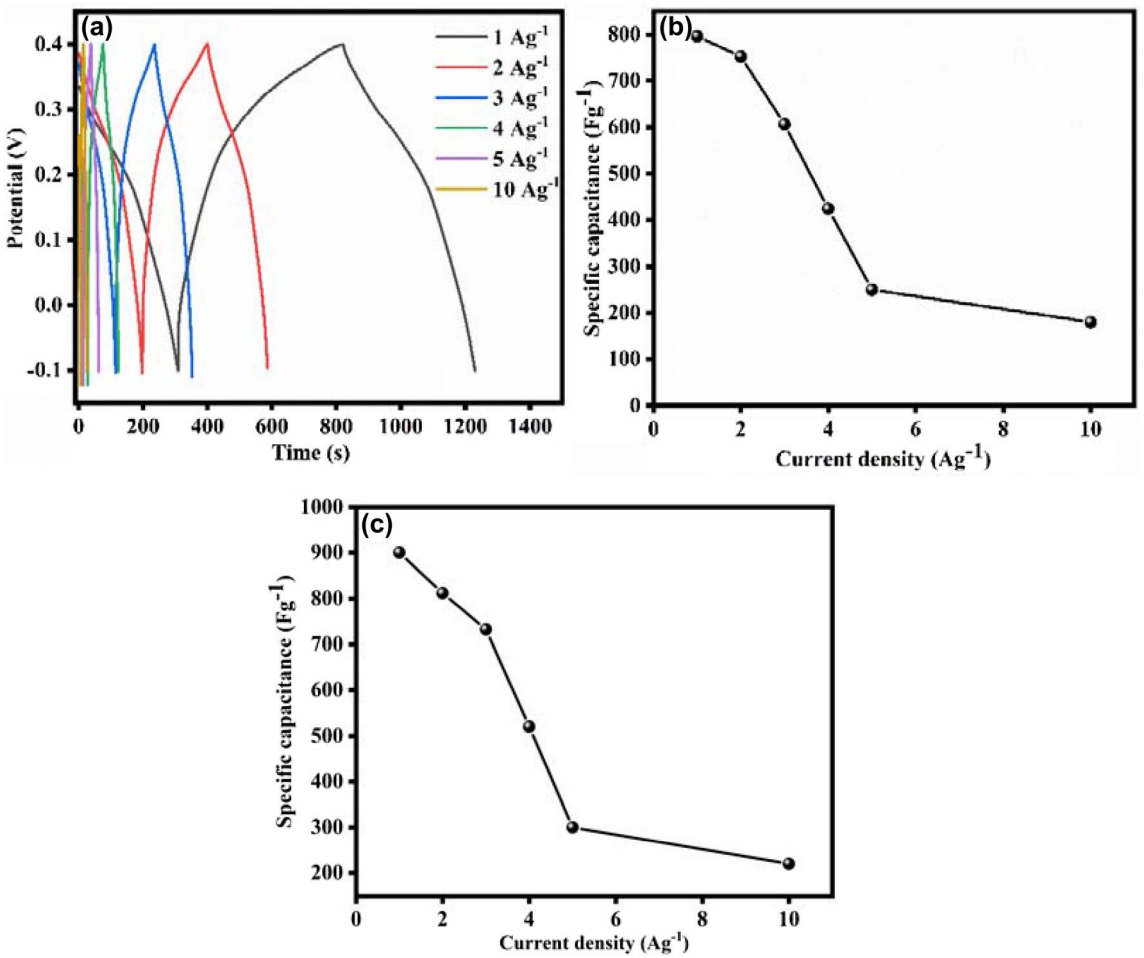

Fig.6 **a** Chronopotentiometric analysis of COM-4 material, **b** Specific capacitance versus current density of discharge current and **c** Specific capacitance versus current density of charge current

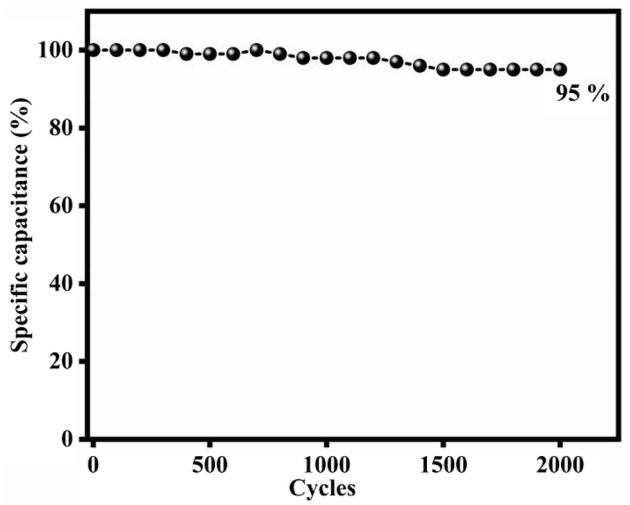

Fig. 7 Cyclic stability analysis of COM-4 material at a scan rate of 100 mVs^{-1} for 2000 continues cycle

capacitance and superior cyclic stability suggest that the cobalt molybdate dihydrate is a potential electrode for supercapacitor energy storage devices.

References

1. H. Peng, G. Ma, J. Mu, K. Sun, Z. Lei, Low-cost and high energy density asymmetric supercapacitors based on polyaniline nanotubes and MoO_3 nanobelts. J. Mater. Chem. A. **2**, 10384–10388 (2014). https://doi.org/10.1039/c4ta01899k
2. X. Li, X. Li, G. Wang, X. Wang, J. Ji, Flexible supercapacitor based on MnO_2 nanoparticles via electrospinning. J. Mater. Chem. A. **1**, 10103–10106 (2013). https://doi.org/10.1039/c3ta11727h
3. R. Zou, K. Xu, T. Wang, G. He, Q. Liu, X. Liu, Z. Zhang, J. Hu, Chain-like $NiCo_2O_4$ nanowires with different exposed reactive planes for high-performance supercapacitors. J. Mater. Chem. A. **1**, 8560–8566 (2013). https://doi.org/10.1039/c3ta11361b
4. L.Y. Chen, J.L. Kang, Y. Hou, P. Liu, T. Fujita, A. Hirata, M.W. Chen, High-energy-density nonaqueous MnO_2@nanoporous gold based supercapacitors. J. Mater. Chem. A. **1**, 9202–9207 (2013). https://doi.org/10.1039/c3ta11480e

5. K. Xu, W. Li, Q. Liu, B. Li, X. Liu, L. An, Z. Chen, R. Zou, J. Hu, Hierarchical mesoporous $NiCo_2O_4$@MnO_2 core-shell nanowire arrays on nickel foam for aqueous asymmetric supercapacitors. J. Mater. Chem. A. **2**, 4795–4802 (2014). https://doi.org/10.1039/c3ta14647b
6. D.H. Nagaraju, Q. Wang, P. Beaujuge, H.N. Alshareef, Two-dimensional heterostructures of V_2O_5 and reduced graphene oxide as electrodes for high energy density asymmetric supercapacitors. J. Mater. Chem. A. **2**, 17146–17152 (2014). https://doi.org/10.1039/c4ta03731f
7. H.Y. Li, K. Jiao, L. Wang, C. Wei, X. Li, B. Xie, Micelle anchored in situ synthesis of V_2O_3 nanoflakes@C composites for supercapacitors. J. Mater. Chem. A. **2**, 18806–18815 (2014). https://doi.org/10.1039/c4ta04062g
8. D. Cai, D. Wang, B. Liu, L. Wang, Y. Liu, H. Li, Y. Wang, Q. Li, T. Wang, Three-dimensional Co_3O_4@NiMoO4 core/shell nanowire arrays on Ni foam for electrochemical energy storage. ACS Appl. Mater. Interf. **6**, 5050–5055 (2014). https://doi.org/10.1021/am500060m
9. J. Wang, J. Chang, L. Wang, J. Hao, One-step and low-temperature synthesis of $CoMoO_4$ nanowire arrays on Ni foam for asymmetric supercapacitors. Ion. Kiel. **24**, 3967–3973 (2018). https://doi.org/10.1007/s11581-018-2552-0
10. Y. Cao, W. Li, K. Xu, Y. Zhang, T. Ji, R. Zou, $MnMoO_4{\cdot}4H_2O$ nanoplates grown on a Ni foam substrate for excellent electrochemical properties. J. Mater. Chem. A Mater. Energy Sustain. **2**, 20723–20728 (2014). https://doi.org/10.1039/C4TA04019H
11. L. Hou, H. Hua, S. Liu, G. Pang, C. Yuan, Surfactant-assisted hydrothermal synthesis of ultrafine $CoMoO_4{\cdot}0.9H_2O$ nanorods towards high-performance supercapacitors. New J. Chem. **39**, 5507–5512 (2015). https://doi.org/10.1039/c5nj00746a
12. W. Li, X. Wang, Y. Hu, L. Sun, C. Gao, C. Zhang, H. Liu, M. Duan, Hydrothermal synthesized of $CoMoO_4$ microspheres as excellent electrode material for supercapacitor. Nanoscale Res. Lett. **13**, 1–10 (2018). https://doi.org/10.1186/s11671-018-2540-3
13. H. Long, T. Liu, W. Zeng, Y. Yang, S. Zhao, $CoMoO_4$ nanosheets assembled 3D-frameworks for high-performance energy storage. Ceram. Int. **44**, 2446–2452 (2018). https://doi.org/10.1016/j.ceramint.2017.10.216
14. J. Wang, S. Wang, J. Chang, X. Jin, One pot preparation of $CoMoO_4$ nanowires covered by $CoMoO_4$ nanosheets for application in asymmetric supercapacitors. J. Mater. Sci. Mater. Electron. (2020). https://doi.org/10.1007/s10854-020-04604-z
15. R. Ramkumar, M. Minakshi, Fabrication of ultrathin $CoMoO_4$ nanosheets modified with chitosan and their improved performance in energy storage device. Dalt. Trans. **44**, 6158–6168 (2015). https://doi.org/10.1039/c5dt00622h
16. M. Mandal, D. Ghosh, S. Giri, I. Shakir, C.K. Das, Polyaniline-wrapped 1D $CoMoO_4{\cdot}0.75H_2O$ nanorods as electrode materials for supercapacitor energy storage applications. RSC Adv. **4**, 30832–30839 (2014). https://doi.org/10.1039/c4ra03399j
17. I. Shaheen, K.S. Ahmad, C. Zequine, R.K. Gupta, A. Thomas, M.A. Malik, Organic template-assisted green synthesis of $CoMoO_4$ nanomaterials for the investigation of energy storage properties. RSC Adv. **10**, 8115–8129 (2020). https://doi.org/10.1039/c9ra09477f
18. K. Xu, J. Chao, W. Li, Q. Liu, Z. Wang, X. Liu, R. Zou, J. Hu, $CoMoO_4{\cdot}0.9H_2O$ nanorods grown on reduced graphene oxide as advanced electrochemical pseudocapacitor materials. RSC Adv. **4**, 34307–34314 (2014). https://doi.org/10.1039/c4ra04827j
19. L.Q. Mai, F. Yang, Y.L. Zhao, X. Xu, L. Xu, Y.Z. Luo, Hierarchical $MnMoO_4$/$CoMoO_4$ heterostructured nanowires with enhanced supercapacitor performance. Nat. Commun. **2**, 381 (2011). https://doi.org/10.1038/ncomms1387
20. P. Villa, F. Trifiro, I. Pasquon, Study of the interaction between $CoMoO_4$ and Al_2O_3 by raman spectroscopy. React. Kinet. Catal. Lett. **1**, 341–344 (1974). https://doi.org/10.1007/BF02070904
21. G.K. Veerasubramani, K. Krishnamoorthy, S. Radhakrishnan, N.J. Kim, S.J. Kim, Synthesis, characterization, and electrochemical properties of $CoMoO_4$ nanostructures. Int. J. Hydrogen Energy. **39**, 5186–5193 (2014). https://doi.org/10.1016/j.ijhydene.2014.01.069
22. S.H. Kazemi, M. Tabibpour, M.A. Kiani, H. Kazemi, An advanced asymmetric supercapacitor based on a binder-free electrode fabricated from ultrathin $CoMoO_4$nano-dandelions. RSC Adv. **6**, 71156–71164 (2016). https://doi.org/10.1039/c6ra05703a
23. D. Guo, H. Zhang, X. Yu, M. Zhang, P. Zhang, Q. Li, T. Wang, Facile synthesis and excellent electrochemical properties of $CoMoO_4$ nanoplate arrays as supercapacitors. J. Mater. Chem. A. **1**, 7247–7254 (2013). https://doi.org/10.1039/c3ta10909g
24. D.T. Dam, T. Huang, J.M. Lee, Ultra-small and low crystalline $CoMoO_4$ nanorods for electrochemical capacitors. Sustain. Energy Fuels **1**, 324–335 (2017). https://doi.org/10.1039/c6se00025h
25. J. Candler, T. Elmore, B.K. Gupta, L. Dong, S. Palchoudhury, R.K. Gupta, New insight into high temperature driven morphology reliant $CoMoO_4$ flexible supercapacitors. New J. Chem. **39**, 6108–6116 (2015). https://doi.org/10.1039/c5nj00446b